

# Study of chirally motivated low-energy $K^-$ optical potentials

A. Cieplý<sup>a,b</sup>, E. Friedman<sup>a</sup>, A. Gal<sup>a</sup>, J. Mareš<sup>b</sup>

<sup>a</sup>*Racah Institute of Physics, The Hebrew University, Jerusalem 91904, Israel*

<sup>b</sup>*Nuclear Physics Institute, 25068 Řež, Czech Republic*

## Abstract

The  $K^-$  optical potential in the nuclear medium is evaluated self consistently from a free-space  $K^-N$   $t$  matrix constructed within a coupled-channel chiral approach to the low-energy  $\bar{K}N$  data. The chiral-model parameters are fitted to a select subset of the low-energy data *plus* the  $K^-$  atomic data throughout the periodic table. The resulting attractive  $K^-$  optical potentials are relatively ‘shallow’, with central depth of the real part about 55 MeV, for a fairly reasonable reproduction of the atomic data with  $\chi^2/N \approx 2.2$ . Relatively ‘deep’ attractive potentials of depth about 180 MeV, which result in other phenomenological approaches with  $\chi^2/N \approx 1.5$ , are ruled out within chirally motivated models. Different physical data input is required to distinguish between shallow and deep  $K^-$  optical potentials. The  $(K_{\text{stop}}^-, \pi)$  reaction could provide such a test, with exclusive rates differing by over a factor of three for the two classes of potentials. Finally, forward  $(K^-, p)$  differential cross sections for the production of relatively narrow deeply bound  $K^-$  nuclear states are evaluated for deep  $K^-$  optical potentials, yielding values considerably lower than those estimated before.

*PACS:* 21.65.+f; 24.10.Ht; 36.10.Gv

*Keywords:* Low energy  $K^-p$  data;  $K^-$  atoms;  $K^-$  optical potentials;  $K^-$  nuclear states;  $(K_{\text{stop}}^-, \pi)$ ,  $(\pi^+, K^+)$  and  $(K^-, p)$  reactions

Corresponding author: E. Friedman,  
Tel: +972 2 658 4667, FAX: +972 2 658 6347,  
E mail: elifried@vms.huji.ac.il

November 9, 2018

## I. INTRODUCTION

There is a considerable interest in exploring the behavior of antikaons in nuclei and in dense nuclear matter [1]. The issues at stake concern the possibility of witnessing precursor phenomena, or even the onset, of kaon condensation in dense nuclear matter, as realized in heavy-ion collisions (see Ref. [2] and references cited therein) or in neutron stars (see Ref. [3] for a recent review). At present, the main evidence for a strong in-medium modification of the  $\bar{K}N$  interaction is due to the enhanced production of  $K^-$  mesons observed in subthreshold and near-threshold heavy-ion collisions in the KaoS experiments at GSI [4–6]. The extrapolation of the  $\bar{K}$  nucleus interaction from standard nuclear density and zero temperature to the higher densities and temperatures which are relevant for the above phenomena is of course model dependent. Nonetheless, direct information on the  $\bar{K}$  nucleus interaction at standard nuclear density and at zero temperature is extremely valuable and studies along these lines are therefore desirable. Unfortunately, even in this regime the situation is not clear cut at present.

Systematic data bearing on the  $\bar{K}$  nucleus interaction near threshold are almost exclusively limited to the strong-interaction shifts and widths of  $K^-$  atomic levels throughout the periodic table [7]. Although the ‘atomic’  $K^-$  meson probes mostly regions of low nuclear density, the wealth of these data largely compensates in producing an effective constraint on the extrapolation to higher densities. The calculations existing to date for the  $\bar{K}$  nucleus interaction at threshold essentially give two different predictions for the depth of the  $K^-$  nucleus potential at nuclear matter density. The phenomenological density dependent (DD) optical potential fits to the kaonic atom data [8,9], and the relativistic mean field (RMF) model calculations by Friedman et al. [10], describe the data quantitatively very well, producing a deeply attractive potential ( $-\text{Re } V_{\text{opt}}(\rho_0) \approx 150 - 200 \text{ MeV}$ ). In contrast, chirally inspired models of the  $\bar{K}N$  interaction, due to Weise and collaborators [11,12] and due to Oset and Ramos [13], give very good fits to the low energy scattering and reaction data in the strangeness  $S = -1$  meson-baryon coupled channel sector and to the  $K^-p$  capture from rest branching ratios, but generally do not describe well the atomic data. Recently, following a suggestion by Lutz [14], the  $K^-$  optical potential has been evaluated *self consistently* within such models [15,16], yielding qualitatively reasonable fits to kaonic atoms [17]. Self consistency means that the outcome  $K^-$  optical potential should be accounted for in the in-medium  $K^-$  propagator that generates it within the appropriate scattering integral equation. These calculations predict a relatively shallow attractive potential ( $-\text{Re } V_{\text{opt}}(\rho_0) \approx 40 - 60 \text{ MeV}$ ). Very recently, Baca et al. [18] improved significantly the fit to the atomic data by adding to the self consistent microscopic optical potential of Ramos and Oset [15] a phenomenological  $s$ -wave ‘ $t\rho$ ’ term of a moderate size (about 30% increase of the real part attraction, but 50% decrease of the imaginary part absorption). However, this improvement was achieved at the cost of losing the direct connection of the optical potential to the chirally inspired microscopic model of the  $\bar{K}N$  interaction.

In the present paper, we aim at preserving the above mentioned connection by showing that reasonable parameters of the chirally motivated microscopic model of the  $\bar{K}N$  interaction can be found such that the low-energy  $\bar{K}N$  data plus the  $K^-$  atomic data are fitted *simultaneously*. This is accomplished in Section II, where the  $K^-$  optical potential providing the atomic fit is constructed self consistently from the in-medium  $\bar{K}N$   $t$  matrix. This

in-medium quantity reduces to the free-space  $t$  matrix of the chirally motivated model as the density goes to zero. The calculations presented in Section II lead to a relatively shallow potential,  $\text{Re } V_{\text{opt}}(\rho_0) \approx -55$  MeV. This depth is quite similar to that found in Ref. [18], but the imaginary part derived in the present work differs substantially from theirs. The quality of the  $K^-$  atomic fit provided by our optical potential is superior.

The vast difference in potential depths between the phenomenological and the more microscopic approaches inevitably brings up the question whether at all, and to what extent, the  $K^-$  atom data contain unambiguous information on the  $\bar{K}$  nuclear potential at nuclear-matter densities. Our experience leads us to believe that the behavior of the optical potential at densities about  $\rho_0$  is primarily determined by the functional form, or by the theoretical model used for the extrapolation from the low-density region which is more directly connected to the  $K^-$  atom data. Furthermore, a related question is whether there exists any experimental procedure for deciding which extrapolation is physically valid. This question is addressed in the present work by showing that the outcome of  $K^-$  initiated reactions at low energy is sensitive to the wavefunction of the  $K^-$  meson inside the nucleus, where different optical potentials produce noticeably different wavefunctions. As an example, we discuss in Section III the  $(K_{\text{stop}}^-, \pi)$  reaction into specific hypernuclear states, demonstrating that the production cross sections are quite sensitive to the  $K^-$  nucleus optical potential.

Several authors [19,20] have drawn attention to  $K^-$  *nuclear* states bound by a very deep potential, similar to the best-fit DD potential of Friedman et al. [8,9]. The deepest states, bound by over 100 MeV, are blocked from decaying by the two-body mode  $\bar{K}N \rightarrow \pi\Sigma$  and their width could then be reduced to about 10 MeV. If a deeply bound state of this kind is identified experimentally, it will provide evidence for a deep  $K^-$  optical potential. In Section IV we evaluate the  $(K^-, p)$  forward cross sections for production of such deeply bound  $K^-$  *nuclear* states. Our evaluation yields considerably lower values than the estimates made by Kishimoto [19] for this reaction at 1 GeV/c.

## II. OPTICAL POTENTIALS FOR KAONIC ATOMS

### A. Empirical potentials based on $\bar{K}N$ amplitudes

$K^-$ -nucleus ‘microscopic’ optical potentials, i.e. potentials constructed from  $K^-p$  and  $K^-n$  scattering amplitudes as function of the local density, have recently been discussed by Baca, García-Recio and Nieves in connection with deeply bound kaonic atom states [18]. In this model the amplitudes are calculated self consistently within a chiral approach [15] and the optical potential is then constructed by multiplying these amplitudes by the corresponding proton and neutron densities. It was shown [18] that such potentials yield marginally acceptable fits to kaonic atom data and that phenomenological modifications of the potential lead to much improved fits to the data. We begin the present section by adopting a similar approach.

The interaction of a  $K^-$  meson with the nucleus in a kaonic atom is described by the Klein-Gordon equation of the form:

$$\left[ \nabla^2 - 2\mu(B + V_{\text{opt}} + V_c) + (V_c + B)^2 \right] \psi = 0 \quad (\hbar = c = 1) \quad , \quad (1)$$

where  $B$  is the complex binding energy and  $V_c$  is the finite-size Coulomb interaction of the hadron with the nucleus, including vacuum-polarization terms. Equation (1) assumes that the optical potential  $V_{\text{opt}}$  behaves as a Lorentz scalar. It is given by a ‘ $t(\rho)\rho$ ’ form:

$$2\mu V_{\text{opt}}(r) = -4\pi\left(1 + \frac{\mu}{M}\right)[a_{K^-p}(\rho)\rho_p(r) + a_{K^-n}(\rho)\rho_n(r)] \quad (2)$$

where  $M$  is the nucleon mass,  $\mu$  is the  $K^-$ -nucleus reduced mass,  $a_{K^-p}$  and  $a_{K^-n}$  are the  $K^-p$  and  $K^-n$  threshold scattering amplitudes evaluated at a nuclear matter density  $\rho = \rho_p + \rho_n$ , and  $\rho_p(r)$  and  $\rho_n(r)$  are the proton and neutron density distributions. The degree of success of any given potential in reproducing the experimental results for kaonic atoms is represented by the values of  $\chi^2$ , defined in the usual way. However, comparing the values of  $\chi^2$  achieved in the present work (see below) with those of Baca et al. [18], one notes that our values are higher. The reason for that is most likely the fact that we use the experimental values for the yields of ‘upper’ levels [9] whereas Baca et al. seem to use the *derived* widths. It is easy to see that when the experimental accuracy is not high, the two definitions of the corresponding  $\chi^2$  may lead to very different  $\chi^2$  values. The use of the measured quantities in the definition of the  $\chi^2$  function rather than derived quantities is the more appropriate way.

Applying the amplitudes of Ramos and Oset [15] without any free parameter leads to  $\chi^2 = 300$  or  $\chi^2/N$  ( $\chi^2$  per point) of 4.62. This value should be compared with  $\chi^2/N = 1.49$  obtained for a phenomenological potential [9] satisfying the low-density theorem constraint. The depths of the potentials at the center of a typical nucleus such as Ni are 44 and 54 MeV for the real and imaginary parts, respectively, compared to 187 and 71 MeV respectively for the phenomenological potential. In order to improve the fit to the data we followed Baca et al. [18] and added a phenomenological ‘ $t\rho$ ’ term to the potential. Another possibility is to apply some scaling factors to the input amplitudes. In order to preserve the predictions of the chirally motivated model in the isospin zero sector where the strongly coupled channels produce the  $\Lambda(1405)$  resonance, we have applied scaling factors  $s_R$  and  $s_I$  only to the isospin 1 combination of the  $K^-p$  and  $K^-n$  amplitudes. More specifically, we have

$$a_{I=0} = 2a_{K^-p} - a_{K^-n}, \quad a_{I=1} = a_{K^-n}, \quad (3)$$

and then we set

$$a'_{I=1} = s_R \text{Re } a_{K^-n} + i s_I \text{Im } a_{K^-n} \quad (4)$$

and derive the modified scattering amplitudes as

$$a'_{K^-n} = a'_{I=1}, \quad a'_{K^-p} = \frac{1}{2}(a_{I=0} + a'_{I=1}). \quad (5)$$

Table I summarizes the results obtained using the input amplitudes, with or without adding a ‘ $t\rho$ ’ term and with or without introducing scaling factors  $s$ . Also included in the table are similar results for the amplitudes of Schaffner-Bielich et al. [16]. Rather poor fits to the data are obtained when the potentials are constructed from the input amplitudes. The fits improve significantly when an empirical ‘ $t\rho$ ’ potential is added, but the resulting total potential is not unique, namely, potentials giving similar values of  $\chi^2$  may differ by

a factor of 2-3 in the nuclear interior. For the Ramos and Oset [15] input amplitudes, we essentially confirm the depths originally found in Ref. [18] upon applying this procedure. Further improvements in the fits are found when scaling factors, as defined by Eq. (5), are included. The values of  $\chi^2/N$  may approach the best value obtained with phenomenological potentials [7] but the required scaling factors are likely to be unphysical.

## B. $\bar{K}N$ scattering amplitudes in the nuclear medium

Here we follow the chirally motivated model of Ref. [11] for  $\bar{K}N$  scattering and reactions near threshold. The  $\Lambda(1405)$  subthreshold resonance is generated in this model dynamically by solving coupled Lippmann-Schwinger equations for the  $t_{ij}$  elements of the  $t$  matrix in terms of the input chiral potentials  $v_{ij}$ . The six coupled meson-baryon channels included in this model are  $K^-p$ ,  $\bar{K}^0n$ ,  $\pi^0\Lambda$ ,  $\pi^+\Sigma^-$ ,  $\pi^0\Sigma^0$  and  $\pi^-\Sigma^+$ . The use of a nonrelativistic formalism is justified for energies close to the  $\bar{K}N$  threshold in accordance with the aims of the present paper.

Applying the coupled-channel model to the calculation of the *in-medium*  $t(\rho)$  matrix, the density dependence of the  $\bar{K}$  optical potential  $t_{\bar{K}N}(\rho)\rho$  can be traced to the propagation of the  $\Lambda(1405)$  resonance in the nuclear medium. Waas et al. [12], following Koch [21], demonstrated that Pauli blocking of the intermediate nucleon is primarily responsible for the transition from a repulsive  $t_{\bar{K}N}(\rho = 0)$ , consistently with the subthreshold  $\Lambda(1405)$ , to an attractive  $t_{\bar{K}N}(\rho)$  in the nuclear interior, as required by the  $K^-$ -atomic data. Later, Lutz [14] stressed the importance of including the kaon self energy within a self consistent calculation, and Ramos and Oset [15] provided a comprehensive calculation of this kind including also pion, nucleon and hyperon self energies.

We extend the calculations of Refs. [11,12] by including  $\bar{K}$  and  $N$  self energies. In this approach, the chirally motivated coupled-channel potentials are taken in a separable form

$$v_{ij}(k, k') = \frac{C_{ij}}{f_\pi^2} \beta_i \beta_j g_i(k^2) g_j(k'^2), \quad g_j(k) = \frac{1}{1 + (k/\alpha_j)^2}, \quad (6)$$

where the momenta  $k$  and  $k'$  refer to the meson-baryon c.m. system in the  $i$  and  $j$  channels, respectively, and the relativistic flux normalization factors  $\beta_i$  are defined by

$$\beta_i = \sqrt{\frac{1}{2\omega_i} \frac{M_i}{E_i}}, \quad (7)$$

with  $\omega_i$ ,  $M_i$  and  $E_i$  denoting the meson energy, the baryon mass and energy in the c.m. system of channel  $i$ . The coupling matrix  $C_{ij}$  is determined by chiral SU(3) symmetry and includes terms up to second order in the meson c.m. kinetic energies (see Ref. [11] for more details). Finally, the parameter  $f_\pi = 94.5$  MeV represents the pseudoscalar meson decay constant, and the inverse range parameters  $\alpha_i$  were fitted to the low energy  $\bar{K}N$  data in Ref. [11]. Their values are

$$\begin{aligned} \alpha_{K^-p} &= \alpha_{\bar{K}^0n} = 757.8 \text{ MeV}, \\ \alpha_{\pi^0\Lambda} &= 300 \text{ MeV}, \\ \alpha_{\pi^+\Sigma^-} &= \alpha_{\pi^0\Sigma^0} = \alpha_{\pi^-\Sigma^+} = 448.1 \text{ MeV}. \end{aligned} \quad (8)$$

The elementary amplitudes corresponding to the potentials (6) are of the form

$$f_{ij}(k, k'; E) = -\frac{1}{4\pi f_\pi^2} \sqrt{\frac{M_i M_j}{E^2}} g_i(k^2) g_j(k'^2) \left[ (1 - C \cdot G(E))^{-1} \cdot C \right]_{ij} , \quad (9)$$

where the meson-baryon propagator  $G(E)$  is diagonal in the channel indices  $i$  and  $j$  and is given by

$$G_i(E; \rho) = \frac{1}{f_\pi^2} \frac{M_i}{E} \int_{\Omega_i(\rho)} \frac{d^3p}{(2\pi)^3} \frac{g_i^2(p^2)}{k_i^2 - p^2 - \Pi_i(\omega_i, E_i, \mathbf{p}; \rho) + i0} . \quad (10)$$

Here the integration domain  $\Omega_i(\rho)$  is limited by the Pauli principle in the  $\bar{K}N$  channels,  $\rho$  denotes the nuclear density and  $k_i$  is the on-shell c.m. momentum in channel  $i$ , such that  $\omega_i^2 = m_i^2 + k_i^2$ ,  $E_i^2 = M_i^2 + k_i^2$ , and  $E = E_i + \omega_i$  is the total energy. In the denominator of the Green's function (10) we have included the meson plus baryon self energy  $\Pi_i$ . For simplicity, we neglect the self energy corrections in the pion-hyperon channels, expecting their effect on the  $\bar{K}N$  channels to be secondary to the primary effect of including the  $\bar{K}$  and nucleon self energies [16]. However, the pion self-energy effect was found nonnegligible in Ref. [15] and this point deserves further study.

The self energy term  $\Pi$  in the c.m.  $\bar{K}N$  channels, close to threshold, is expressed in terms of the more familiar self energies of the antikaon and the nucleon as follows:

$$\Pi = \frac{\mu_{KN}}{m_K} \Pi_{\bar{K}} + \frac{\mu_{KN}}{M} \Pi_N , \quad (11)$$

where  $\mu_{KN}$  is the  $\bar{K}N$  reduced mass,  $\Pi_{\bar{K}} = 2m_K V_{\text{opt}}^{\bar{K}}$  in terms of the  $\bar{K}$  optical potential given in Eq. (2), and  $\Pi_N = 2M V_{\text{opt}}^N$  in terms of the nucleon optical potential which in the present work was taken in the form

$$V_{\text{opt}}^N = V_0 \frac{\rho}{\rho_0} , \quad (12)$$

where  $\rho_0 = 0.17 \text{ fm}^{-3}$ . For the nucleon optical potential we used  $V_0 = (-60 - i10) \text{ MeV}$ . The real part is consistent with mean-field potentials used in nuclear structure calculations. The strength of the imaginary part is adopted from proton-nucleus scattering analysis [22].

It should be noted that when the meson and baryon self energies are turned off, our model reduces to the in-medium model presented in Ref. [12]. It is also obvious that the same applies for zero density. This means that we are able to reproduce the free-space threshold branching ratios and cross sections fitted in Ref. [11]. Below we show that a satisfactory description of these free-space low-energy data can also be achieved in a simultaneous fit of the model parameters to these data and to the  $K^-$ -atomic data.

### C. Fits to kaonic atoms and $K^-p$ data

The chiral model presented above was applied in  $\chi^2$  fits to  $K^-$ -atomic data and to representative low energy  $K^-p$  data. The latter consist of the three accurately measured threshold branching ratios [23]

$$\gamma = \frac{\Gamma(K^-p \rightarrow \pi^+\Sigma^-)}{\Gamma(K^-p \rightarrow \pi^-\Sigma^+)}, \quad R_c = \frac{\Gamma(K^-p \rightarrow \text{charged})}{\Gamma(K^-p \rightarrow \text{all})}, \quad R_n = \frac{\Gamma(K^-p \rightarrow \pi^0\Lambda)}{\Gamma(K^-p \rightarrow \text{neutral})}, \quad (13)$$

plus four  $K^-p$  - initiated cross sections at 110 MeV/c to the channels other than the  $\pi^0\Lambda$  and  $\pi^0\Sigma^0$  channels for which the quality of data is inferior. The adopted experimental values of the cross sections [23–25]

$$\sigma(K^-p \rightarrow K^-p), \quad \sigma(K^-p \rightarrow \bar{K}^0n), \quad \sigma(K^-p \rightarrow \pi^+\Sigma^-), \quad \sigma(K^-p \rightarrow \pi^-\Sigma^+), \quad (14)$$

as well as the measured branching ratios  $\gamma$ ,  $R_c$  and  $R_n$  are listed in Table II. The values calculated for the above seven quantities are also listed, using (i) the original parameterization of Ref. [12] (denoted ‘no SC’) which did not account for  $\bar{K}$  and  $N$  self energies; and (ii) the present model (denoted ‘ $V_N$ , full’) which was fitted to both the free-space  $K^-p$  data (13,14) as well as to the  $K^-$  atomic data, including self consistently  $\bar{K}$  and  $N$  self energies. Table II demonstrates that extending the fit to include the atomic data does not spoil the good agreement with the experimental low energy  $K^-p$  data.

Table III summarizes the results obtained within the present approach. The upper two rows involve no fits to the atomic data; the  $\bar{K}$  self energy is not included in the in-medium calculation pertaining to the first row (‘no SC’), whereas this self energy is included self consistently in the in-medium amplitudes of the calculation of the second row (‘SC’). The nucleon self energy is excluded in both calculations. The  $\chi^2$  value for the seven  $K^-p$  data points is of course the same in both calculations which, however, differ markedly in the  $\chi_{\text{atom}}^2$  values with respect to the 65 atomic data points. The calculated  $K^-$  optical potential is made considerably shallower and the description of the atomic data improves upon requiring self consistency, in agreement with Refs. [17,18]. The remaining four rows are for various fits to the 65  $K^-$  atomic data points, some excluding (‘atoms’) and some including (‘full’) the 7 free-space  $K^-p$  data points in the fit, all with the  $\bar{K}$  self energy included self consistently in the in-medium calculation. The last two rows (‘ $V_N$ ’) are for the additional inclusion of the nucleon self-energy optical potential of Eq. (12). The table also specifies the resulting scaling factors which multiply the pseudoscalar meson decay constant  $f_\pi = 94.5$  MeV and the inverse range parameters  $\alpha_i$  of Eq. (8). It is seen that the modification of the free-space model parameters is moderate. Also given are the depths of the real and imaginary potentials at the center of the Ni nucleus. The depth of 55 MeV for the real part (last row in the table) is very close to the corresponding depth found in Ref. [18], but the depth of 60 MeV for the imaginary part is considerably larger than that found there. It is clear from the table that, with relatively small modifications of the chiral-model parameters, it is possible to achieve reasonably good fits to both atomic and free-space data. The best  $\chi_{\text{atom}}^2$  means  $\chi_{\text{atom}}^2/N$  of 2.2, a value which is significantly lower than the value 2.7 corresponding to the hybrid fit of Ref. [18], yet considerably higher than the value 1.5 obtained with best-fit phenomenological potentials [7]. It is therefore again concluded that when a free-space interaction model is used to fit the  $K^-$  atomic data, the quality of the fit is inferior to that achieved with phenomenological fits which are constrained only by the low density theorem.

Figure 1 shows cross sections calculated for six free-space  $K^-p$  initiated reactions in comparison with the data (as compiled in Fig. 1 of Ref. [11]). The results of our full model (‘ $V_N$ , full’) and the free-space calculation (‘no SC’) were chosen for illustration. The cross sections calculated for the other parameterizations of Table III are of a similar quality. It is

emphasized that we obtain equally good fits to the cross sections as well as to the threshold branching ratios even when *only*  $K^-$  atomic data are used in the fit. Moreover, we find that the inclusion of the nucleon self-energy optical potential  $V_{\text{opt}}^N$  plays only a marginal role in the improvement of the fit to the data. Of course, the size and form of  $V_{\text{opt}}^N$  influences considerably the depth of the resulting  $K^-$  nucleus optical potential, as demonstrated in the table.

Figure 2 shows the density dependence of the isospin averaged (effective) threshold scattering amplitude  $a_{\text{eff}} = (3a_{\text{eff}}^{I=1} + a_{\text{eff}}^{I=0})/4$  for three cases selected from Table III: (i) no medium effects beyond Pauli blocking are included (‘no SC’, dashed line); (ii) the self-consistent calculation including the  $\bar{K}$  self energy (‘SC’, dot-dashed line); and (iii) plus including the nucleon self energy (‘ $V_N$ , full’, solid line). The change of the sign of  $\text{Re } a_{\text{eff}}$  from negative to positive corresponds to the transition from an apparently repulsive free-space interaction to an attractive one in the nuclear medium. In the ‘no SC’ model, in which medium modifications are represented only by the Pauli blocking effect, the transition occurs at  $\rho \approx 0.1\rho_0$ . When the  $K^-$  self energy is taken into account, this transition occurs at a lower density,  $\rho \approx 0.05\rho_0$ , and the inclusion of  $V_{\text{opt}}^N$  pushes this transition density even further down. Nevertheless, the free-space ( $\rho = 0$ ) threshold scattering amplitude remains negative even in this case, reflecting the dominance of the  $\Lambda(1405)$   $I = 0$  subthreshold resonance. We note that since the ‘no SC’ and ‘SC’ parameterizations coincide, the low-density limit of  $a_{\text{eff}}$  for these cases is the same, whereas  $a_{\text{eff}}(\rho = 0)$  for the ‘ $V_N$ , full’ parameterization assumes a different value.

Taking the  $K^-$  self energy into account generally leads to a weaker density dependence of the threshold scattering amplitude, both for its real and imaginary parts. This indicates that the  $K^-$  optical potential evaluated within such self consistent models is well approximated by a  $t_{\text{eff}}\rho$  form (where  $t_{\text{eff}} = \text{const.}$ ) over a wide range of densities. A genuine  $\rho$  dependence of  $t_{\text{eff}}$  appears only at very low densities.

The free-space ( $\rho = 0$ ) scattering amplitude  $f_{I=0}$ , as a function of the c.m. energy  $E$ , is shown in Fig. 3. The calculated amplitude for the ‘no SC’ parameterization (first row in Table III, dashed line here) is compared with that for the ‘ $V_N$ , full’ parameterization (last row in Table III, solid line here). The peak of  $\text{Im } f_{I=0}$  is shifted upward by over 10 MeV when the  $K^-$  atom data are included in the fit. These amplitudes, for which the real part changes sign at the energy where the imaginary part peaks, provide a signature of the  $\Lambda(1405)$  subthreshold resonance. We note that a precise reproduction of the  $\Lambda(1405)$  spectral shape requires a more involved calculation than the  $I = 0$   $\bar{K}N - \pi\Sigma$  coupled channel calculation reported in the present work and, therefore, this spectral shape was not used here as a constraint. A new datum that was unavailable to the authors of Refs. [11,12] is the  $K^-p$  scattering length, deduced from the recent measurement of the  $2p \rightarrow 1s$  X ray in kaonic hydrogen [26] and which we too have not included in the fit to the data. Model ‘ $V_N$ , full’ does very well with respect to  $\text{Re } a_{K^-p}$ , but does poorly for the imaginary part. However, the rapid variation of  $\text{Im } f_{I=0}$  near threshold should make it fairly easy to reproduce it by slightly varying the parameters of the present chiral model.

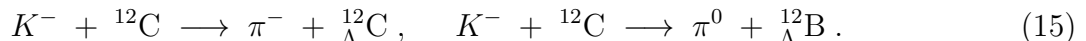
For completeness, we also tested the 10 channel chiral model of Refs. [13,15], including also the  $\eta\Lambda$ ,  $\eta\Sigma^0$ ,  $K^+\Xi^-$ , and  $K^0\Xi^0$  channels. We treated it on the same footing as our 6 channel model, namely a separable form was used for the coupled-channel potentials, and only  $\bar{K}$  and  $N$  self energies were considered. Fitting to the  $K^-$  atom data led to  $\chi^2$  values



comparable to those for the 6 channel model.

### III. STOPPED $K^-$ REACTIONS AS A TEST OF THE $K^-$ NUCLEUS OPTICAL POTENTIAL

In this section we discuss the possibility of testing the  $K^-$  optical potential at threshold by studying  $(K_{\text{stop}}^-, \pi)$  reactions to specific  $\Lambda$  hypernuclear states. The  $(K_{\text{stop}}^-, \pi^-)$  reaction has been used to explore the spectroscopy of  $\Lambda$  hypernuclei (see Ref. [27] for a review). Recently, the use of the complementary  $(K_{\text{stop}}^-, \pi^0)$  reaction was proposed [28] and first results on  $^{12}\text{C}$  are forthcoming [29]. Calculations of  $\Lambda$ -hypernuclear formation rates for  $(K_{\text{stop}}^-, \pi^-)$  reactions were presented by several groups [30–33] within the framework of the distorted wave impulse approximation. The present calculation follows the approach described in Ref. [31]. Our aim is to study the sensitivity of the capture rates to the choice of the  $K^-$  nucleus optical potential, provided the latter was fitted to the  $K^-$  atomic data. Here we limit the discussion to the following  $K^-$  capture-at-rest reactions on  $^{12}\text{C}$ :



The capture rate per stopped  $K^-$  from the  $^{12}\text{C}$  initial state  $i$  to a  $\Lambda$ -hypernuclear final state  $f$ ,  $R_{fi}/K^-$ , is given by [31]

$$R_{fi}/K^- = \frac{q_f \omega_f}{\bar{q}_f \bar{\omega}_f} R(\pi\Lambda) \frac{\int d\Omega_{\mathbf{q}_f} \langle | F_{fi}^{\text{DW}}(\mathbf{q}_f) |^2 \rangle}{4\pi \bar{\rho}_N}, \quad (16)$$

where the fractions  $R(\pi\Lambda)$  are the in-medium branching ratios for  $K^- N \rightarrow \pi\Lambda$  capture at rest, as given in Table I of Ref. [31], and the kinematic factor involving the pion momentum  $q$  and energy  $\omega$  in front of  $R(\pi\Lambda)$  is due to considering the pion final-state phase space with respect to an average closure phase space marked by bars. The product of these two factors for capture on  $^{12}\text{C}$  is 0.074 (for  $R(\pi^- \Lambda)$ )  $\times$  1.456 (for  $q_f \omega_f / \bar{q}_f \bar{\omega}_f$ ), equaling 0.1077 for  $(K_{\text{stop}}^-, \pi^-)$  and half of that, by charge independence, for  $(K_{\text{stop}}^-, \pi^0)$ . The distorted wave (DW) transition amplitude is given by

$$F_{fi}^{\text{DW}}(\mathbf{q}_f) = \int d^3r \chi_{\mathbf{q}_f}^{(-)*}(\mathbf{r}) \rho_{fi}(\mathbf{r}) \Psi_{nLM}(\mathbf{r}) \quad , \quad (17)$$

with  $\rho_{fi}$  denoting the nuclear to hypernuclear transition density matrix element. The brackets  $\langle \dots \rangle$  in Eq. (16) stand for averaging on the initial substates and summing over the final ones. Finally,  $\bar{\rho}_N$  denotes the effective nuclear density available to the capture process,

$$\bar{\rho}_N = \int d^3r \rho_N(r) | \Psi_{nLM}(\mathbf{r}) |^2 \quad , \quad (18)$$

where  $\rho_N(r)$  is the appropriate nucleon (proton or neutron) density and  $\Psi_{nLM}(\mathbf{r})$  is the  $K^-$  wavefunction in the  $nL$  orbit from which the  $K^-$  meson is captured.

The radial wavefunctions for nucleons in  $^{12}\text{C}$ , and for the  $\Lambda$  hyperon in  $^{12}_\Lambda\text{C}$  and  $^{12}_\Lambda\text{B}$ , were generated by solving the Schrödinger equation for a real Woods-Saxon potential with a diffusivity parameter  $a = 0.6$  fm. The depth  $V_0$  was adjusted separately for each baryon orbit to yield the observed binding energies. The proton Coulomb potential due to the nuclear

core charge distribution was also included. The single-particle wavefunctions thus obtained were used in the calculation of  $\rho_{fi}(\mathbf{r})$  for the DW amplitude (17) and also for constructing  $\rho_N(r)$  in Eq. (18). The value of the radius parameter  $r_0$  was chosen such that for protons the r.m.s. radius of  $\rho_p$  was equal to the r.m.s. radius of the charge distribution after unfolding from the latter the proton size. As already observed in Ref. [31], since the baryonic radial wavefunctions that enter the capture rate calculation are nodeless and real, the resulting calculated rates (16) are considerably less sensitive to variations in these wavefunctions than to similar model variations of the pion and  $K^-$  wavefunctions.

To generate the pion DW  $\chi_{\mathbf{q}_f}^{(-)}$  in Eq. (17) we used the measured pion elastic scattering angular distribution for  $\theta_{\text{cm}} < 90^\circ$  at 162 MeV on  $^{12}\text{C}$  [34] in order to fit the standard pion-nucleus optical potential

$$2\mu_\pi V_{\text{opt}}^\pi = 4\pi[-(1 + \frac{\mu_\pi}{M})b_0\rho(r) + (1 + \frac{\mu_\pi}{M})^{-1}c_0\nabla\rho(r) \cdot \nabla] \quad (19)$$

for which  $\chi$  solves the Klein Gordon equation. We have managed to improve considerably the fits of Ref. [31], getting as low as  $\chi^2/N = 3.2$  for the following values of parameters:

$$b_0 = (-0.24 + i 0.18) m_\pi^{-1}, \quad c_0 = (0.20 + i 0.31) m_\pi^{-3}. \quad (20)$$

In addition to the chirally motivated  $K^-$  optical potential discussed in the previous section, several  $K^-$  initial-state wavefunctions were generated using the density-dependent form of the  $K^-$  optical potential [9]

$$2\mu V_{\text{opt}} = -4\pi(1 + \frac{\mu}{M}) \left[ a + B \left( \frac{\rho(r)}{\rho(0)} \right)^\gamma \right] \rho(r), \quad (21)$$

where the notation follows the ' $t(\rho)\rho$ ' form, Eq. (2). For these optical potentials, the energy shifts and widths of the  $2p$  and  $3d$  levels in kaonic  $^{12}\text{C}$ , and the corresponding wavefunction  $\Psi_{nLM}(\mathbf{r})$ , were then obtained by solving the Klein-Gordon equation (1). Four different optical potentials, ordered according to their central depth, are listed in Table IV. The 'chiral' potential corresponds to the relatively shallow potential of the present work. The deep potential 'DD' was obtained by Friedman et al. [9] fitting the parameters  $B$  and  $\gamma$ , with the value of  $a$  held fixed at the empirical  $K^-N$  scattering length, so that the potential (21) satisfies the low-density limit. The potential ' $t_{\text{eff}}$ ' was obtained for  $B = 0$  as the best-fit  $t_{\text{eff}}\rho$  solution for the standard density independent version of  $V_{\text{opt}}$ . Since the above potentials were obtained within *global* fits to the available  $K^-$ -atomic data, they do not necessarily reproduce precisely the experimental data on kaonic  $^{12}\text{C}$  [35], and for this reason we added in Table IV another potential (' $\tilde{t}_{\text{eff}}$ ') designed primarily to fit these latter data.

The calculated capture rates per  $K^-$ , Eq. (16), are shown in Table V for the production of the  $1^-$  hypernuclear ground states off  $^{12}\text{C}$ , assuming atomic capture fractions  $f_p = 0.23$  and  $f_d = 0.77$  according to a cascade calculation by Batty [36] which fits the absolute and relative X-ray intensities for  $^{12}\text{C}$ . It is clear that the deeper the  $K^-$  optical potential is, the lower the calculated rate becomes. This pattern is caused by the strong-interaction bound  $d$  state generated by all but the 'chiral' potentials, as may be recognized by the repulsive shift (see Table IV) they impose on the  $3d$  atomic state. By orthogonality, the atomic wavefunction acquires then *extra* nodes within the nucleus, thus causing substantial

cancelations in the DW amplitude (17). This effect was extensively studied in Ref. [31] for  $K^-$  capture from atomic  $p$  states in  $^{12}\text{C}$ , but for the dominant capture from atomic  $d$  states there was no similar effect since the relatively shallow potentials considered there (similar to the present ‘chiral’ potential) did not produce strong-interaction bound  $d$  states. All the calculated rates shown in the table are lower than the measured values. Tamura et al. [27] report a rate of  $(0.98 \pm 0.12) \times 10^{-3}$  per stopped  $K^-$  for the production of  $^{12}_{\Lambda}\text{C}$ . This value is still four times larger than our highest calculated value, that for the ‘chiral’ potential. The largest uncertainty in our calculation is due to the pion distortion effects which we estimate as about 10%, so the discrepancy between experiment and calculation cannot be resolved at present. Therefore, although the  $K^-$  capture from rest reaction does exhibit significant sensitivity to the type of  $V_{\text{opt}}$ , it cannot yet be used to exclude potentials which are permissible from the point of view of fitting  $K^-$  atomic data.

#### IV. PRODUCTION OF $K^-$ NUCLEAR BOUND STATES

$K^-$  nuclear bound states are expected, generally, to have widths of order  $\Gamma \approx -2 \text{Im}V_{\text{opt}}(\rho_0) \approx 100$  MeV. However, for particularly deep states, bound by over 100 MeV, the dominant two-body pionic decay modes of the  $\bar{K}N$  system get blocked so that these states stand a chance of being resolved in some appropriate production reactions. If such relatively narrow deeply bound states are ever observed, then the  $K^-$  nucleus optical potential must be sufficiently deep. Kishimoto [19] has suggested to search for deeply bound  $K^-$  nuclear states using the forward  $(K^-, p)$  reaction in which the incoming  $K^-$  meson knocks out in the forward direction a bound proton from the target nucleus, while itself getting captured in a nuclear bound state generated by  $V_{\text{opt}}$ . This is equivalent to a backward ( $\theta = \pi$ )  $K^-p$  elastic scattering, and will be denoted by  $K^-p \rightarrow pK^-$ . In this section we calculate, more rigorously than done in Ref. [19], the relevant production cross sections at laboratory momentum  $p_L = 1$  GeV/c.

The forward differential  $(K^-, p)$  laboratory cross section on a nuclear target, due to a single-particle transition from the proton  $(n_p, l_p)$  shell to the  $K^-$   $(n_{K^-}, l_{K^-})$  bound state in the residual nucleus, is expressed in the distorted-wave (DW) impulse approximation [30] in terms of the Fermi-averaged forward  $K^-p \rightarrow pK^-$  laboratory cross section:

$$\left( \frac{d\sigma(0^\circ)}{d\Omega_L} \right)^{(K^-, p)} = \alpha \left( \frac{d\sigma(0^\circ)}{d\Omega_L} \right)^{K^-p \rightarrow pK^-} P_{n_p l_p \rightarrow n_{K^-} l_{K^-}}^{\text{DW}} . \quad (22)$$

Here,  $\alpha$  is a kinematical factor which accounts for the transformation from the two-body laboratory system to the many-body laboratory system [37] and  $P_{n_p l_p \rightarrow n_{K^-} l_{K^-}}^{\text{DW}}$  is an effective proton number for the transition  $n_p l_p \rightarrow n_{K^-} l_{K^-}$  given by

$$P_{n_p l_p \rightarrow n_{K^-} l_{K^-}}^{\text{DW}} = \frac{1}{(2l_p + 1)} \sum_{m_{K^-} = m_p} \sum_{j_p = l_p \pm 1/2} S_{j_p} | \langle (nlm)_{K^-} | \chi_p^{(-)*}(\mathbf{r}) \chi_{K^-}^{(+)}(\mathbf{r}) | (nlm)_p \rangle_{j_p} |^2 . \quad (23)$$

In Eq. (23),  $S_{j_p}$  is the  $j_p$  proton pickup spectroscopic factor in the target (with a maximum value of  $(2j_p + 1)$ ) and the suffix  $j_p$  attached to the matrix element stands for a possible

$j_p$  dependence of the bound proton radial wavefunction. We note that Eqs. (22,23) are equivalent to Eq. (3.15) of Ref. [38] for the  $(K^-, \pi^-)$  reaction. For the distorted waves  $\chi(\mathbf{r})$  we use the eikonal approximation, retaining only the exponential attenuation factor,

$$\chi_p^{(-)*}(\mathbf{r}) \chi_{K^-}^{(+)}(\mathbf{r}) \approx \exp(iqz) \exp\left(-\frac{\bar{\sigma}}{2}T(b)\right), \quad (24)$$

where  $q$  is the momentum transfer, purely longitudinal at  $0^\circ$ , with  $\bar{\sigma}$  denoting an average  $\bar{K}N$  and  $pN$  total cross section, and where the nuclear thickness function  $T(b)$  is defined by

$$T(b) = \int_{-\infty}^{\infty} \rho(r) dz \quad \left( \int T(b) d^2b = A \right). \quad (25)$$

Here  $\mathbf{b}$  is the impact-parameter coordinate in the plane perpendicular to the direction of the forward momentum transfer  $\mathbf{q}$ . The functions  $T(b)$  were evaluated numerically, using realistic density distributions for  $\rho(r)$ .

We have calculated the DW expression (23) for the forward  $(K^-, p)$  reaction at incoming momentum  $p_L = 1$  GeV/c on  $^{12}\text{C}$  and  $^{28}\text{Si}$ , to the  $K^- 1s$  state generated by the  $K^-$  nucleus DD optical potential. The imaginary part of  $V_{\text{opt}}$  was reduced to 12% of its nominal strength in order to account for the reduced phase space for  $K^-$  absorption, assuming no change in the in-medium properties of the decay products. The results given below are rather insensitive to the precise amount of this reduction. By approximating the  $K^-$  and proton bound-state wavefunctions by harmonic oscillator (HO) wavefunctions, the matrix elements in Eq. (23) reduce to a one dimensional numerical integration in the variable  $b$ , as follows:

$$P_{1p_p \rightarrow 1s_{K^-}}^{\text{DW}} = \left( \frac{\tilde{b}^8}{b_{K^-}^3 b_p^5} \right) S_{p_{3/2}} \frac{1}{6} (\tilde{b}q)^2 \exp\left(-\frac{1}{2}(\tilde{b}q)^2\right) |G_0(\bar{\sigma})|^2 \quad (26)$$

for  $^{12}\text{C}$ , and

$$P_{1d_p \rightarrow 1s_{K^-}}^{\text{DW}} = \left( \frac{\tilde{b}^{10}}{b_{K^-}^3 b_p^7} \right) S_{d_{5/2}} \frac{1}{15} \exp\left(-\frac{1}{2}(\tilde{b}q)^2\right) |G_2(\bar{\sigma}) - G_0(\bar{\sigma})(1 - (\tilde{b}q)^2/2)|^2 \quad (27)$$

for  $^{28}\text{Si}$ , with the distorted-wave integrals

$$G_k(\bar{\sigma}) = \int_0^\infty 2t^{k+1} \exp(-t^2) \exp\left(-\frac{\bar{\sigma}}{2}T(\tilde{b}t)\right) dt, \quad G_k(\bar{\sigma} = 0) = 1, \quad k = 0, 2. \quad (28)$$

The mean HO size parameter  $\tilde{b}$  is defined by

$$\frac{1}{\tilde{b}^2} = \frac{1}{2} \left( \frac{1}{b_{K^-}^2} + \frac{1}{b_p^2} \right) \quad (29)$$

in terms of the  $K^-$  and proton HO size parameters.

The accuracy of this approximation is estimated to incur errors of up to 10% in the calculated cross sections. In order to provide a concrete and useful check, we have also calculated the forward  $(\pi^+, K^+)$  reaction cross sections at  $p_L = 1.04$  GeV/c on the same targets as above, leading to the known  $1s$   $\Lambda$  hypernuclear ground states in the residual nuclei. The momentum transfer characterizing this reaction is quite similar to that in the

$(K^-, p)$  reaction. The calculation of cross sections for the production of  $\Lambda$  1s bound states is identically the same as for the  $K^-$  1s bound states, upon the replacement of bound protons in Eqs. (22,23) by bound neutrons. The results of this calculation are shown in Table VI, with  $b_\Lambda$  and  $b_n$  standing for the  $\Lambda$  and neutron HO size parameters, respectively, where the size parameter  $b$  is identified by the  $\exp(-r^2/2b^2)$  exponential factor of the HO wavefunction. The ratio of effective neutron number for the DW calculation,  $N^{\text{DW}}$ , to the effective neutron number for the plane-wave (PW) calculation,  $N^{\text{PW}}$ , is also given, as a measure of the effect of absorption. The input parameters  $\alpha$  ( $d\sigma(0^\circ)/d\Omega_L$ ) = 0.5 mb/sr for  $\pi^+n \rightarrow K^+\Lambda$ ,  $\bar{\sigma} = 27.5$  mb and  $S_{j_n} = 2j_n + 1$  for the valent  $p_{3/2}$  and  $d_{5/2}$  neutron orbits in  $^{12}\text{C}$  and  $^{28}\text{Si}$ , respectively, are the same as in the eikonal calculation of Motoba et al. [39], which did not use the HO approximation, for the  $(\pi^+, K^+)$  reaction. The agreement between the latter calculation and the present one, as shown in Table VI, is very reasonable, inspiring confidence in the present results for the  $(K^-, p)$  reaction (Table VII). We note that the preliminary value for the  $(\pi^+, K^+)$  forward cross section on  $^{12}\text{C}$  in experiment E336 at KEK [40] is  $15 \pm 1$   $\mu\text{b/sr}$ .

The forward  $(K^-, p)$  differential cross sections listed in Table VII were calculated assuming a value of 3.6 mb/sr for the factor  $\alpha$  ( $d\sigma(0^\circ)/d\Omega_L$ ) in front of  $P^{\text{DW}}$  on the r.h.s. of Eq. (22). This value is based on the measured two-body  $K^-p$  c.m. backward cross section  $1.7 \pm 0.1$  mb/sr at  $p_L = 1$  GeV/c [41], on the value  $\alpha = 0.69$  appropriate to this kinematics, and on an estimated Fermi-average reduction factor of 0.59 due to the peaking of the two-body elastic  $K^-p$  backward cross section at 1 GeV/c as function of the incoming momentum, following the procedure outlined in Ref. [38]. For the distortion, using the value  $\bar{\sigma} = 40$  mb [19], the suppressive effect on the forward  $(K^-, p)$  cross sections is considerably stronger than for the  $(\pi^+, K^+)$  reaction. This is partly due also to the extremely small spatial extension of the  $K^-$  wavefunction which restricts the  $(K^-, p)$  reaction to the denser nuclear region where absorption prevails. In contrast, the extension of the  $\Lambda$  wavefunction in the  $(\pi^+, K^+)$  reaction is substantially larger. The effect of absorption gets stronger with the atomic number of the target nucleus, as seen clearly from Table VII by comparing the results for Si with those for C. Another reason for the fast decrease of the calculated cross section with increasing  $A$  is the gradual increase of the momentum transfer  $q$  in the  $(K^-, p)$  reaction due to the increased binding of the  $K^-$  meson. This is just opposite to the trend observed in Table VI for the  $(\pi^+, K^+)$  reaction, where  $q$  gradually decreases as function of  $A$  due to the increased binding of the  $\Lambda$  hyperon.

Finally, we comment on the marked disagreement between the results of the present calculations and the estimates due to Kishimoto [19] shown in Table VII. The wide range of estimated cross-section values in Ref. [19] reflects primarily the dependence of the PW expressions Eqs. (26,27) on the HO size parameter  $b_{K^-}$ . The smaller  $b_{K^-}$  is, the higher the PW cross section becomes. However, the lowest value of  $b_{K^-}$  assumed there,  $b_{K^-} = b_N/8^{1/4}$ , was erroneously chosen instead of the considerably larger value  $b_{K^-} = b_N/2^{1/4}$  that the correct HO scaling argument leads to. This should narrow appreciably the range of values for the PW cross section. Furthermore, it appears inconceivable that just one value for the distortion factor  $P^{\text{DW}}/P^{\text{PW}}$ , as quoted from Ref. [19] in Table VII, can be considered representative for the whole range of  $b_{K^-}$  values assumed by Kishimoto. For this matter, the smaller  $b_{K^-}$  is, the more suppressive is the effect of the distortion. The dependence on  $b_{K^-}$  is rather strong and thus largely cancels the opposite trend of the PW calculation as explained above. The overall dependence on  $b_{K^-}$  is therefore much weaker than one is led to

believe in Ref. [19]. As for the absolute scale of the suppression provided by the distortion factors  $P^{\text{DW}}/P^{\text{PW}}$ , we find it inconceivable that Kishimoto's suppression effects are even weaker than we and other works [39] find for the  $(\pi^+, K^+)$  reaction. The present results call for extreme caution when contemplating  $(K^-, p)$  experiments aimed at identifying deeply bound  $K^-$  nuclear states.

## V. SUMMARY AND CONCLUSIONS

At present the best tool for exploring the  $K^-$  interactions in the nuclear medium at low energy is the study of strong interaction effects in kaonic atoms. Extrapolating this interaction to higher densities, as encountered in astrophysical scenarios, must rely on some theory, beyond the phenomenological potential that fits the data very well. The prime aim of the present work was to see how far one can go in bringing microscopic approaches to the  $K^-$ -nucleus interaction into agreement with the  $K^-$  atomic data. The chirally motivated coupled channel approach to the  $\bar{K}N$  interaction, which is quite successful in reproducing all the low energy  $K^-p$  data, was chosen as a starting point. Earlier attempts to use this approach indicated poor agreement with the atomic data and only by introducing self consistency into the theory it became possible to achieve barely acceptable fits. Empirical modifications of the interaction managed to improve the fits to the atomic data, but at the cost of losing contact with the underlying  $\bar{K}N$  interaction model, thus making questionable any extrapolation of such optical potentials to higher densities.

In the present work we addressed the problem by requiring *simultaneous* fits to atomic and  $K^-p$  data within the chirally motivated coupled channel approach, including self consistently the self energies of the kaons and, in some cases, of the nucleons. It was found that minor modifications of parameters of this theory led to good agreement with the atomic data while maintaining the good agreement with the  $K^-p$  data. In fact, we found that one can fit only the atomic data and still not lose the good fit to the  $K^-p$  data. The best value of  $\chi^2$  per point obtained here for the  $K^-$  atomic data is 2.2, compared to 1.5 for the best-fit phenomenological potential. Nevertheless, the fits of the self consistent chirally motivated coupled channel potentials are quite good.

The depth of the real part of the  $K^-$  nucleus potential is also of prime interest in connection with the possibility of kaon condensation in collapsing stars. Deep (180 MeV) potentials were found in the phenomenological analysis, whereas shallow (55 MeV) potentials are found in the framework of models which require the  $K^-$  optical potential to be derived self consistently. It seems impossible to reconcile the phenomenological potentials with the present microscopic potentials both in terms of depth and in terms of values of  $\chi^2$ . Since the depth of the  $K^-$ -nucleus optical potential cannot be resolved by studying only kaonic atoms, we briefly discussed the ability to do so with the help of reactions initiated by stopped  $K^-$  mesons. The mechanism behind it is the sensitivity of the DW integrals to the depth of the real part of the  $K^-$  potential, due to the node structure of the wavefunction, which is quite different from each other for deep and for shallow potentials. It was demonstrated that  $\Lambda$ -hypernuclear ground-state production rates calculated for the  $(K_{\text{stop}}^-, \pi)$  reactions on carbon differ by more than a factor of 3 between the different potential depths mentioned above. Unfortunately, these calculated rates are still several times smaller than the measured ones [27], so that these reactions cannot yet be used to reach a definite conclusion on the

depth of the  $K^-$  nucleus optical potential near threshold. However, it is plausible that by studying the effect of the  $K^-$  potential on the pion spectrum of the capture reactions, one could reach more definite conclusions.

Finally, we addressed the possibility of identifying deeply bound  $K^-$  *nuclear* states in the forward ( $K^-, p$ ) reaction on nuclear targets. Using the very deep DD potential [9], we calculated a cross section as large as  $47 \mu\text{b}/\text{sr}$  at  $p_L = 1 \text{ GeV}/c$  for the production of the  $1s$   $K^-$  bound state on  $^{12}\text{C}$ . This  $K^-$  nuclear ‘ground state’ is bound by about 120 MeV, which strips it off most of the phase space for its dominant pionic decay modes, so that its residual width could become as small as 10-20 MeV. In contrast, using the HO size parameter  $b_{K^-} = 1.22 \text{ fm}$  from Table VII, the first excited ( $1p$ ) state is estimated to lie about  $\hbar\omega \approx 50 \text{ MeV}$  higher and, therefore, it should be much wider and hardly observable. We verified this estimate by an explicit calculation. If the  $K^-$  nuclear potential is not of the ‘deep’ kind, it may still accommodate bound states, but these will be very wide, judging from the depth of  $\text{Im } V_{\text{opt}}$  found in this work for the ‘shallow’ chirally motivated potentials. We calculated the  $1s_{K^-}$  bound state production cross section also on  $^{28}\text{Si}$ , finding it to be about 8 times smaller than on  $^{12}\text{C}$ . This rules out using medium-weight or heavy targets for this reaction. Not much different production cross sections should be expected at lower incoming momentum, say at  $600 \text{ MeV}/c$ . Our calculated cross sections, tested for the kinematically similar ( $\pi^+, K^+$ ) reaction, are substantially lower than those estimated by Kishimoto [19].

This research was partially supported by the Israel Science Foundation (E.F. and A.G., grant No. 171/98) and by the Grant Agency of the Czech Republic (A.C. and J.M., grant No. 202/00/1667). A.C. and J.M. acknowledge the hospitality of the Hebrew University. We thank A. Ramos and J. Schaffner-Bielich for discussions and for communicating the scattering amplitudes of Refs. [15,16] respectively.

## REFERENCES

- [1] A. Ramos et al., arXiv:nucl-th/0101031, Nucl. Phys. A (in press).
- [2] W. Cassing and E. Bratkovskaya, Phys. Rep. 308 (1999) 65.
- [3] H. Heiselberg and M. Hjorth-Jensen, Phys. Rep. 328 (2000) 237.
- [4] F. Laue et al., Phys. Rev. Lett. 82 (1999) 1640.
- [5] F. Laue et al., Eur. Phys. J. A9 (2000) 397.
- [6] M. Menzel et al., Phys. Lett. B 495 (2000) 26.
- [7] C.J. Batty, E. Friedman and A. Gal, Phys. Rep. 287 (1997) 385.
- [8] E. Friedman, A. Gal and C.J. Batty, Phys. Lett. B 308 (1993) 6.
- [9] E. Friedman, A. Gal and C.J. Batty, Nucl. Phys. A 579 (1994) 518.
- [10] E. Friedman, A. Gal, J. Mareš and A. Cieplý, Phys. Rev. C 60 (1999) 024314.
- [11] N. Kaiser, P.B. Siegel and W. Weise, Nucl. Phys. A 594 (1995) 325.
- [12] T. Waas, N. Kaiser and W. Weise, Phys. Lett. B 365 (1996) 12; 379 (1996) 34.
- [13] E. Oset and A. Ramos, Nucl. Phys. A 635 (1998) 99.
- [14] M. Lutz, Phys. Lett. B 426 (1998) 12.
- [15] A. Ramos and E. Oset, Nucl. Phys. A 671 (2000) 481.
- [16] J. Schaffner-Bielich, V. Koch and M. Effenberger, Nucl. Phys. A 669 (2000) 153.
- [17] S. Hirenzaki, Y. Okumura, H. Toki, E. Oset and A. Ramos, Phys. Rev. C 61 (2000) 055205.
- [18] A. Baca, C. García-Recio and J. Nieves, Nucl. Phys. A 673 (2000) 335.
- [19] T. Kishimoto, Phys. Rev. Lett. 83 (1999) 4701.
- [20] Y. Akaishi and T. Yamazaki, Nucl. Phys. A 684 (2001) 409c.
- [21] V. Koch, Phys. Lett. B 337 (1994) 7.
- [22] L.G. Arnold, B.C. Clark, R.L. Mercer and P. Schwandt, Phys. Rev. C 23 (1981) 1949.
- [23] A.D. Martin, Nucl. Phys. B 179 (1981) 33; and earlier references cited therein.
- [24] J. Ciborowski et al., J. Phys. G 8 (1982) 13.
- [25] D. Evans et al., J. Phys. G 9 (1983) 885.
- [26] T.M. Ito et al., Phys. Rev. C 58 (1998) 2366.
- [27] H. Tamura, R.S. Hayano, H. Outa and T. Yamazaki, Prog. Theor. Phys. Suppl. 117 (1994) 1.
- [28] Brookhaven AGS Exp. E907 (1994), spokespersons: E.V. Hungerford and J.C. Peng.
- [29] R.E. Chrien and A. Rusek, private communication (2001).
- [30] J. Hüfner, S.Y. Lee and H.A. Weidenmüller, Phys. Lett. 49 B (1974) 409; Nucl. Phys. A 234 (1974) 429.
- [31] A. Gal and L. Klieb, Phys. Rev. C 34 (1986) 956.
- [32] H. Bando and T. Motoba, Prog. Theor. Phys. 76 (1986) 1321; K. Itonaga, T. Motoba and H. Bando, Prog. Theor. Phys. 84 (1990) 291.
- [33] A. Matsuyama and K. Yazaki, Nucl. Phys. A 477 (1988) 673.
- [34] J. Piffaretti et al., Phys. Lett. 71 B (1977) 324; H.A. Thiessen et al., LAMPF Report No. LA-7607-PR (1978); C.J. Harvey et al., LAMPF Report No. LA-UR-84-1732 (1984).
- [35] G. Backenstoss, J. Egger, H. Koch, H.P. Povel, A. Schwitter and L. Tauscher, Nucl. Phys. B 73 (1974) 189.
- [36] C.J. Batty, private communication (1995).
- [37] C.B. Dover, L. Ludeking and G.E. Walker, Phys. Rev. C 22 (1980) 2073.



- [38] E.H. Auerbach, A.J. Baltz, C.B. Dover, A. Gal, S.H. Kahana, L. Ludeking and D.J. Milner, *Ann. Phys. [NY]* 148 (1983) 381.
- [39] T. Motoba, H. Bando, R. Wünsch and J. Žofka, *Phys. Rev. C* 38 (1988) 1322.
- [40] O. Hashimoto, presentation at the 1995-2000 KEK PS Review (Dec. 2000).
- [41] B. Conforto et al., *Nucl. Phys. B* 105 (1976) 189.

TABLES

TABLE I. Kaonic atom optical potentials using two sets of self consistent in-medium  $\bar{K}N$  scattering amplitudes, with or without adding a complex ‘ $t\rho$ ’ potential, and with or without scaling the  $I = 1$  amplitude.  $V_R$  and  $V_I$  refer to the depth of  $V_{\text{opt}}$  for Ni.

amplitude	$t_R$ (fm)	$t_I$ (fm)	$s_R$	$s_I$	$\chi^2/N$	$V_R$ (MeV)	$V_I$ (MeV)
Ref. [15]	0	0	1	1	4.62	-44	-54
	0.11±0.02	-0.20±0.02	1	1	2.73	-58	-23
	0	0	2.0±0.2	0.9±0.2	3.08	-61	-52
	1.17±0.11	-0.03±0.15	-0.5±0.5	0.96±0.54	2.00	-170	-49
Ref. [16]	0	0	1	1	12.7	-34	-62
	1.0±0.1	0.26±0.06	1	1	2.46	-159	-95
	0	0	4.5±0.3	5.7±0.7	2.82	-134	-116
	2.9±0.4	-2.8±0.8	-6.1±1.7	34±9	1.49	-204	-82

TABLE II. Calculated branching ratios (13) at the  $K^-p$  threshold, and total cross sections (in mb) for selected  $K^-p$  reactions (14) at incident momentum  $p_L = 110$  MeV/c, for the ‘no SC’ and ‘ $V_N$ , full’ parameterizations of Table III. Also shown are the experimental data.

	$\gamma$	$R_c$	$R_n$	$\sigma(K^-p)$	$\sigma(\bar{K}^0n)$	$\sigma(\pi^+\Sigma^-)$	$\sigma(\pi^-\Sigma^+)$
‘no SC’	2.383	0.667	0.171	93.2	41.2	60.1	32.3
‘ $V_N$ , full’	2.347	0.669	0.198	94.5	38.0	71.2	42.0
exp. [23–25]	2.36±0.04	0.664±0.011	0.189±0.015	92 ± 8	29 ± 6	64 ± 10	29 ± 6

TABLE III. Values of  $\chi^2$ , optical potentials and scaling factors for the present chiral model.  $\chi_{\text{atom}}^2$  refer to the  $K^-$  atom 65 data points and  $\chi_{\text{T}}^2$  is the sum of the former and the  $\chi^2$  for the 7 data points for the free-space  $K^-p$  data.  $V_{R,I}$  are the optical potential values at the center of the Ni nucleus and  $V_N$  stands for fits where the nucleon optical potential is included. The scaling factors  $f$  and  $\alpha(j)$  multiply the parameters  $f_\pi$  and  $\alpha_j$ , respectively, of the coupled channel model.

model	$\chi_{\text{T}}^2$	$\chi_{\text{atom}}^2$	$V_R$ (MeV)	$V_I$ (MeV)	$f$	$\alpha(K^-p)$	$\alpha(\bar{K}^0n)$	$\alpha(\pi^0\Lambda)$	$\alpha(\pi\Sigma)$
no SC	1082	1076	-117	-67	1	1	1	1	1
SC	443.1	436.7	-70.6	-85.6	1	1	1	1	1
atoms	169.9	157.2	-66.9	-55.2	1.12±0.05	1.00±0.08	1.21±0.08	1.05±0.17	1.39±0.07
full	165.3	157.5	-66.8	-54.0	1.14±0.05	1.03±0.07	1.24±0.08	1.13±0.16	1.35±0.07
$V_N$ , atoms	156.3	145.4	-56.3	-61.8	1.04±0.04	0.86±0.06	1.07±0.05	1.00±0.14	1.18±0.08
$V_N$ , full	154.0	145.8	-54.9	-60.2	1.06±0.04	0.90±0.06	1.10±0.06	1.08±0.15	1.17±0.07

TABLE IV.  $K^-$  optical potentials and calculated strong-interaction shifts and widths, in eV, for the  $2p$  and  $3d$   $K^-$  atomic levels in  $^{12}\text{C}$ .

$V_{\text{opt}}$	$a$ (fm)	$B$ (fm)	$\gamma$	$\epsilon_{2p}$	$\Gamma_{2p}$	$\epsilon_{3d}$	$\Gamma_{3d}$
chiral	-	-	-	-616	1484	+0.01	0.57
$t_{\text{eff}}$	$0.63 + i0.89$	-	-	-590	1360	-0.01	0.64
$\tilde{t}_{\text{eff}}$	$1.30 + i0.80$	-	-	-605	1731	-0.01	0.85
DD	$-0.15 + i0.62$	$1.65 - i0.06$	0.23	-468	1578	-0.08	0.64
exp. [35]				$-590 \pm 80$	$1730 \pm 150$	-	$0.98 \pm 19$

TABLE V. Calculated capture rates on  $^{12}\text{C}$  per stopped  $K^-$  (in units of  $10^{-3}$ ) to the summed  $p_N \rightarrow s_\Lambda 1^-$  excitations in  $^{12}_\Lambda\text{C}$  and  $^{12}_\Lambda\text{B}$ , for the  $K^-$  optical potentials of Table IV.

final $^A_\Lambda\text{Z}$	chiral	$t_{\text{eff}}$	$\tilde{t}_{\text{eff}}$	DD
$^{12}_\Lambda\text{C}$	0.231	0.169	0.089	0.063
$^{12}_\Lambda\text{B}$	0.119	0.087	0.046	0.032

TABLE VI. Input and results of DWIA eikonal calculations for the forward ( $\pi^+, K^+$ ) reaction cross section (in  $\mu\text{b}/\text{sr}$ ) at incoming momentum  $p_L = 1.04$  GeV/c, see text for details.

target	$B_{1s}^\Lambda$ (MeV)	$q$ (MeV/c)	$b_\Lambda$ (fm)	$b_n$ (fm)	$N^{\text{DW}}/N^{\text{PW}}$ [present]	$(d\sigma(0^\circ)/d\Omega_L)^{(\pi^+, K^+)}$ [present]	Ref. [39]
$^{12}\text{C}$	10.8	335	1.72	1.52	0.237	15.4	17.4
$^{28}\text{Si}$	16.7	322	1.92	1.72	0.132	7.7	8.9

TABLE VII. Input and results of DWIA eikonal calculations for the forward ( $K^-, p$ ) reaction cross section (in  $\mu\text{b}/\text{sr}$ ) at incoming momentum  $p_L = 1$  GeV/c, see text for details.

target	$B_{1s}^{K^-}$ (MeV)	$q$ (MeV/c)	$b_{K^-}$ (fm)	$G_0$	$G_2$	$P^{\text{DW}}/P^{\text{PW}}$ [present]	Ref. [19]	$(d\sigma(0^\circ)/d\Omega_L)^{(K^-, p)}$ [present]	Ref. [19]
$^{12}\text{C}$	122	369	1.22	0.308	—	0.095	0.25	47	100-490
$^{28}\text{Si}$	144	404	1.42	0.183	0.269	0.040	0.16	6.0	35-180

FIGURES

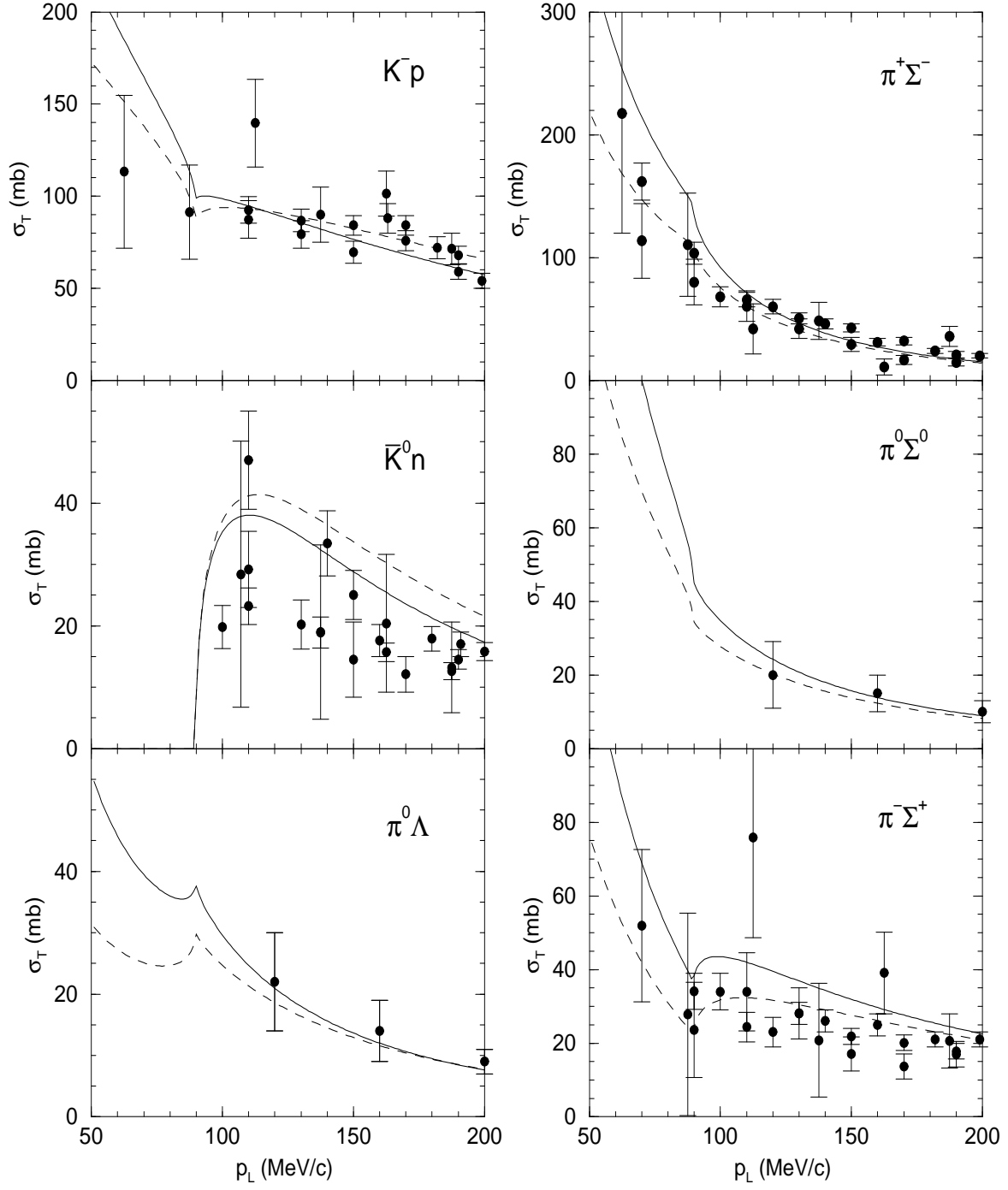


FIG. 1. Cross sections for  $K^-p$  scattering and reactions to the channels indicated in the figure. Results of the full fit (' $V_N$ , full', see Table III), displayed by solid lines, are compared with the available data (see text). Results for the free-space chiral-model parameterization ('no SC') are shown for comparison (dashed lines).

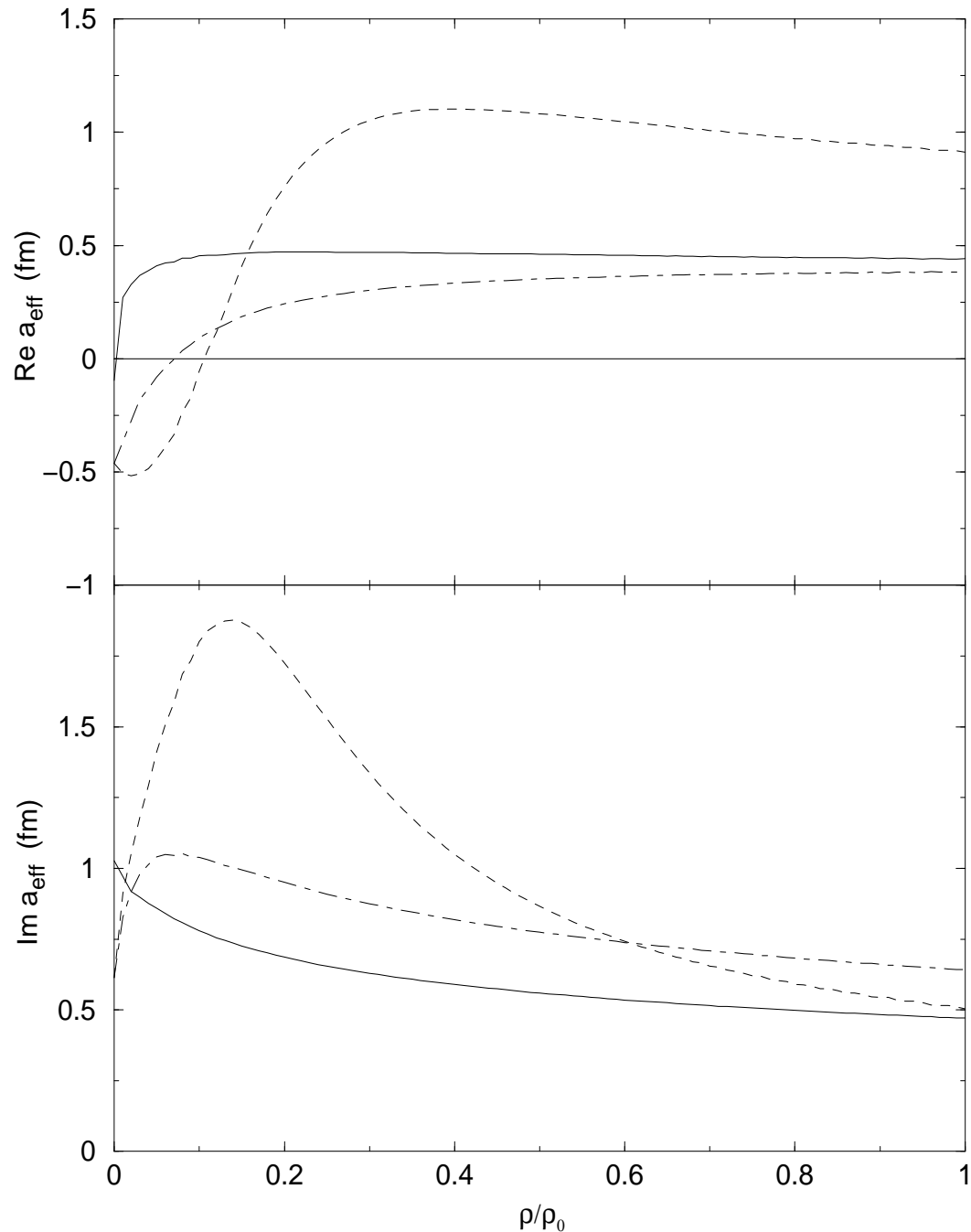


FIG. 2. Real (top) and imaginary (bottom) parts of the isospin-averaged  $K^-N$  (effective) threshold scattering amplitude as function of density  $\rho/\rho_0$ , calculated for the ‘no SC’ (dashed line), ‘SC’ (dot-dashed line) and ‘ $V_N$ , full’ (solid line) chiral-model parameterizations (see Table III).

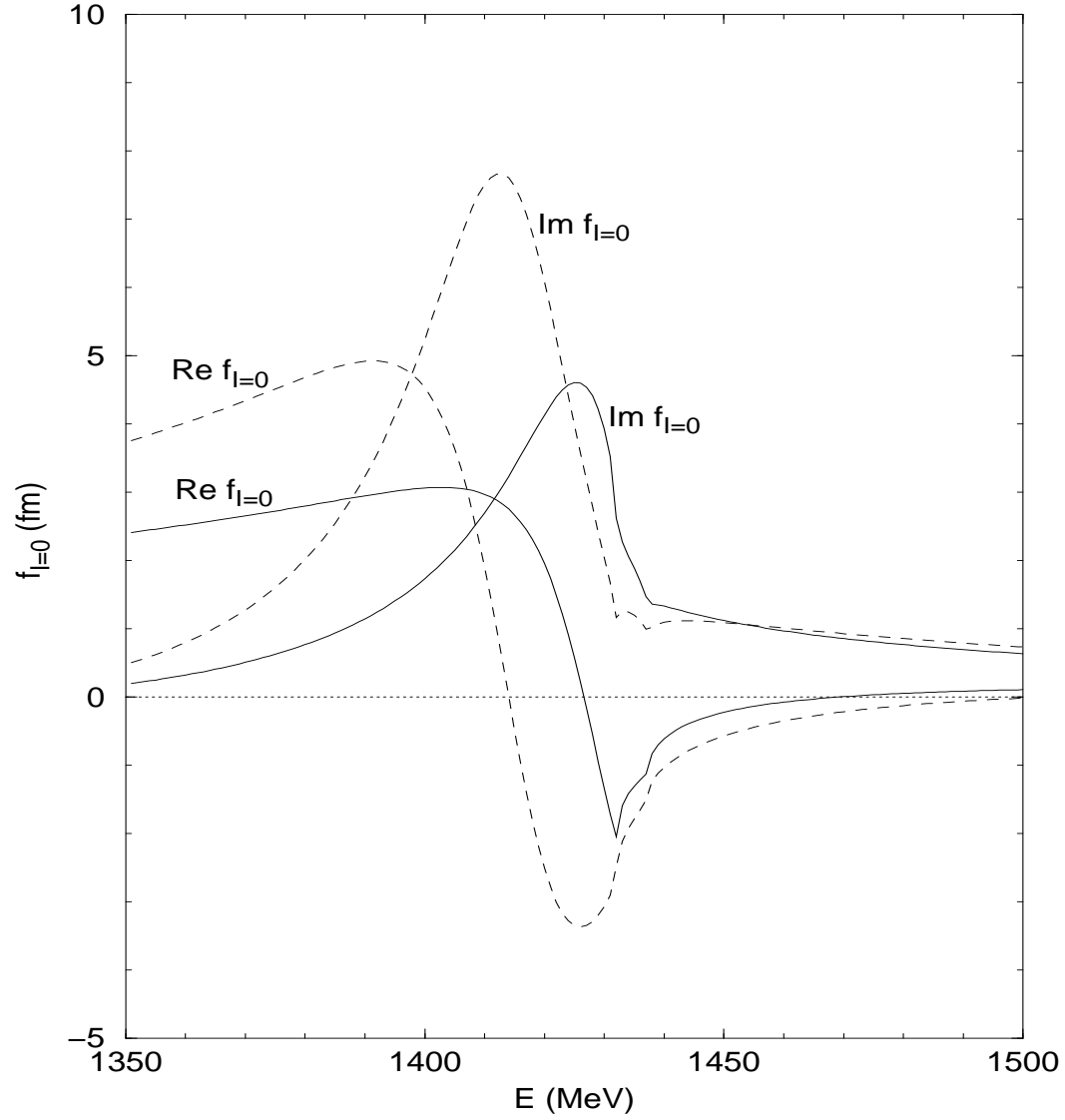


FIG. 3. The  $\bar{K}N$  free-space scattering amplitude  $f_{I=0}$  as function of c.m. energy. Results are presented for the ‘no SC’ (dashed lines) and ‘ $V_N$ , full’ (solid lines) chiral-model parameterizations from Table III.